Published in final edited form as:
Biochemistry. 2013 October 8; 52(40): 7022–7030. doi:10.1021/bi4008726.

Single mutations that redirect internal proton transfer in the *ba*$_3$ oxidase from *Thermus thermophilus*

Irina Smirnova[1,3], **Hsin-Yang Chang**[2], **Christoph von Ballmoos**[1], **Pia Ädelroth**[1], **Robert B. Gennis**[2], and **Peter Brzezinski**[1,*]

[1]Department of Biochemistry and Biophysics, The Arrhenius Laboratories for Natural Sciences, Stockholm University, SE-106 91 Stockholm, Sweden

[2]Department of Biochemistry, University of Illinois at Urbana Champaign, Urbana, Illinois 61801, United States

Abstract

The *ba*$_3$-type cytochrome *c* oxidase from *Thermus thermophilus* is a membrane-bound proton pump. Results from earlier studies have shown that with the *aa*$_3$-type oxidases proton uptake to the catalytic site and "pump site" occur simultaneously. However, with the *ba*$_3$ oxidase the pump site is loaded before proton transfer to the catalytic site because the proton transfer to the latter is slower than with the *aa*$_3$ oxidases. In addition, the timing of formation and decay of catalytic intermediates is different in the two types of oxidases. In the present study, we have investigated two mutant *ba*$_3$ Cyt*c*Os in which residues of the proton pathway leading to the catalytic site as well as the pump site were exchanged, Thr312Val and Tyr244Phe. Even though the *ba*$_3$ Cyt*c*O uses only a single proton pathway for transfer of the substrate and "pumped" protons, the amino-acid residue substitutions had distinctly different effects on the kinetics of proton transfer to the catalytic site and the pump site, respectively. The results indicate that the rates of these reactions can be modified independently by replacement of single residues within the proton pathway. Furthermore, the data suggest that the Thr312Val and Tyr244Phe mutations interfere with a structural rearrangement in the proton pathway that is rate limiting for proton transfer to the catalytic site.

Keywords

cytochrome *c* oxidase; electron transfer; membrane protein; respiration; electrochemical potential; redox reaction; metalloprotein; cytochrome *aa*$_3$

Cytochrome c oxidases (Cyt*c*Os) are terminal enzymes of the membrane-bound respiratory chains in aerobic prokaryotic and eukaryotic organisms. This group of enzymes catalyses sequential reduction of oxygen to water and uses part of the free energy released in this reaction for generation of a transmembrane electrochemical proton gradient. Energy conservation by terminal oxidases occurs via two mechanisms. The electron donor, cytochrome *c*, binds on the positive (*p*) side of the membrane while protons used in the

*Correspondence: peterb@dbb.su.se, fax: +46-8-153679, phone +46 70 609 2642.
[3]Present address: A. N. Belozersky Institute of Physico-Chemical Biology, Moscow State University, Moscow 119899, Russia.

reduction of oxygen to water originate from opposite, negative (*n*) side of the membrane, which results in a charge separation across the membrane. In addition, up to now, all investigated Cyt*c*Os have been shown to energetically link electron transfer to pumping of protons across the membrane, from the *n* to the *p* side (1–5).

The ba_3 Cyt*c*O consists of two main core subunits, I and II, and an additional subunit IIa. Subunit I consists of 13 transmembrane helices and holds heme *b* as well as the catalytic site composed of heme a_3 and Cu_B. A fourth redox site, Cu_A, is located in subunit II. This site acts as the primary electron acceptor, which receives electrons from the water-soluble cytochrome c_{552}. Subunit IIa forms one transmembrane helix, which corresponds to a helix of subunit II of e.g. the *Rhodobacter sphaeroides* Cyt*c*O, however, with opposite polarity (6–18). During turnover, electrons are transferred from Cu_A consecutively to heme *b* and to the catalytic site, which upon reduction binds O_2 that is reduced to water. The protons involved in this reaction are transferred through specific proton-conducting pathways that span the distance between the *n*-side surface and the catalytic site. While the aa_3-type oxidases (from e.g. *R. sphaeroides*, *P. denitrificans* or mitochondria) harbor two functional proton-conducting pathways, D and K, the ba_3 oxidase presumably uses only one pathway, which partly overlaps in space with the Kpathway in the aa_3 Cyt*c*Os (10, 19). This pathway is presumably used for transfer of all protons, including those used for O_2 reduction and those being pumped across the membrane. The results from functional studies, combined with analyses of the ba_3 Cyt*c*O structures (7–10), indicate that the entrance to the K-pathway is near a water molecule (H_2O 146) and a conserved Glu in subunit II (E15(II)). The pathway is defined by a number of polar residues and water molecules that span the distance between solution and the catalytic site (Figure 1a).

The reaction of the reduced ba_3 Cyt*c*O with oxygen has been studied previously upon laser flash photolysis of CO from the ba_3-CO complex in the presence of O_2. The results from these experiments showed that at neutral pH the general reaction sequence is similar to that observed with the aa_3 Cyt*c*Os. However, notable differences were observed in the timing of the individual electron and proton-transfer reactions (Figure 1b) (20–24), which may be related to the 0.5 H^+/e^- pumping stoichiometry of the ba_3 oxidase (25, 26) (compared to 1 H^+/e^- in the aa_3 oxidases studied to date). In brief, in both the aa_3 (here data with the *R. sphaeroides* Cyt*c*O are discussed for comparison, (5, 27)) and ba_3 Cyt*c*Os the reaction is initiated by oxygen binding to the reduced heme a_3 with a time constant of 5–10 μs (at 1 mM O_2). The binding of O_2 is followed in time by electron transfer from heme *b* (heme *a* in aa_3 Cyt*c*O) to the catalytic site with a time constant of ~15 μs or ~40 μs in the ba_3 and aa_3 Cyt*c*Os, respectively (Table 1). This electron transfer results in formation of a state that is called $\mathbf{P_R}$. In the next step, a proton is taken up from solution and the electron at Cu_A equilibrates with heme *b*/*a* with a time constant of ~60 μs and ~90 μs with the ba_3 and aa_3 Cyt*c*Os, respectively. However, while with the aa_3 Cyt*c*O this proton is transferred to the catalytic site to form state **F**, with the ba_3 Cyt*c*O the proton is transferred to a site that is located at a distance from the catalytic site, suggested to be the so-called proton-loading site (PLS) (23). With the aa_3 Cyt*c*O, the fourth electron, accompanied by proton uptake, is transferred to the catalytic site with a time constant of ~1 ms forming the oxidized Cyt*c*O (both the $\mathbf{P_R} \rightarrow \mathbf{F}$ and $\mathbf{F} \rightarrow \mathbf{O}$ reactions are linked in time to proton pumping). With the ba_3

Cyt*c*O the 60-μs proton uptake is followed in time by proton uptake to form the **F** state with a time constant of ~0.8 ms at neutral pH, which is significantly slower than with the aa_3 Cyt*c*O (c.f. ~100 μs). This reaction approximately overlaps in time with transfer of the last electron to the catalytic site and formation of the oxidized Cyt*c*O (state **O**). In other words, the **F** state is not significantly populated with the ba_3 Cyt*c*O. At pH >8 the two processes are separated in time such that formation of **F** and **O** are resolved separately[1]. Thus, the main difference between the reaction sequences for the aa_3 and ba_3 Cyt*c*Os is that while with the former proton uptake to the PLS and the catalytic site are synchronized, with the ba_3 Cyt*c*O the two processes are separated in time; proton transfer to PLS occurs before proton transfer to the catalytic site. Furthermore, while with the aa_3 Cyt*c*O two protons are pumped during O_2 reduction, with the ba_3 Cyt*c*O only one proton is pumped.

To elucidate the mechanism by which the ba_3 Cyt*c*O couples O_2 reduction to proton pumping, we searched for structural modifications in the K pathway analog of the ba_3 Cyt*c*O (10) that could result in specific changes in the kinetics of proton uptake during the reaction steps associated with O_2 reduction. Two such structural modifications are the replacement of Thr312 by a Val residue (T312V) and Tyr244 by a Phe residue (Y244F). The turnover activities of these mutant Cyt*c*Os were <1% and ~15%, respectively, of that of the wild-type Cyt*c*O (~300 s^{-1}). The proton-pumping stoichiometry of the Y244F mutant Cyt*c*O was similar to that of the wild-type Cyt*c*O (the activity of the T312V was too low to allow measurements of proton pumping) (10).

In this work, we show that in these mutant Cyt*c*Os, the first proton was taken up only slightly slower than with the wild-type Cyt*c*O, but the second proton uptake was significantly slowed such that the oxidized state (**O**) was formed slower than state **F** resulting in a temporal separation of the two events. The data indicate that even though the substrate and pumped protons are transferred through a single pathway, the T312V and Y244F substitutions have distinctly different effects on the relative rates of the electron and proton-transfer reactions, which offers insights into the mechanism by which these processes are regulated.

Materials and Methods

Bacterial growth, enzyme purification and characterization

Thermus thermophilus HB8 strain YC 1001 (with a deletion of the *cba* gene and a plasmid with the ba_3 gene with a 6-His-tag at the N-terminus of subunit I) was used for production of cytochrome ba_3 Cyt*c*O. Mutations were introduced as described previously (10, 28). Purification of the recombinant ba_3-Cyt*c*O was performed as described in (23). The ba_3-Cyt*c*O variants at a concentration of 100–150 μM in 5 mM HEPES, pH 8.0, 0.05% DDM were kept at 4°C.

The optical absorbance spectra of both structural variants T312V and Y244F in their oxidized, reduced and in CO-ligated forms were essentially the same as those of the wild-type Cyt*c*O.

Flow-flash experiments

The cytochrome ba_3 sample was prepared in a Thunberg cuvette as described in (29, 30). Briefly, air was replaced by nitrogen on a vacuum line after which the samples were reduced upon addition of 2–3 mM sodium ascorbate and 2 μM of the redox mediator phenazine methosulphate (PMS) in 100 mM HEPES-NaOH or 100 mM KCl (for measurements of proton uptake) and 0.05 % dodecyl-β-D-maltoside (DDM). Then, nitrogen was exchanged for carbon monoxide about one hour before initiation of the experiment. In order to obtain the partially reduced enzyme (3 electrons/enzyme) the samples were supplemented with 30 μM EDTA, air was replaced with nitrogen and then carbon monoxide on the vacuum line. The samples were kept over night in order to reach the three-electron reduced state and 10–30 μM $FeSO_4$ was added. In order to test whether or not the presence of EDTA and $FeSO_4$ had any specific effect on the studied reactions, in part of the experiments ascorbate and PMS were added to fully reduce the Cyt*c*O (with 4 electrons) after completing the experiments with the three-electron reduced Cyt*c*O, and the reaction with O_2 was monitored. No differences were observed compared to the data obtained with the four-electron reduced Cyt*c*O prepared from the oxidized Cyt*c*O as described above.

Flow-flash experiments were performed using a locally modified stopped-flow apparatus (Applied Photophysics, DX-17MV) as described in (31). Briefly, the enzyme-containing solution was mixed with an oxygen-saturated solution at a ratio of 1:5 resulting in a final oxygen concentration of ~1 mM. About 30 ms after mixing the reaction of the enzyme with oxygen was initiated by flash-photolysis of the enzyme-CO complex (10 ns; 200 mJ; 532 nm, Nd-YAG laser, Quantel). The oxidation kinetics were monitored at different wavelengths (see Figure legends). The concentration of the reactive enzyme was calculated from the amplitude of the flash-induced absorbance increase at 445 nm using an absorption coefficient of 67 $mM^{-1}cm^{-1}$ (20).

Proton-uptake measurements

Proton uptake during oxidation of the fully or partially reduced enzyme with oxygen was measured using the pH indicator dye cresol red (pK_a=8.3) at a concentration of 33 μM (after mixing). The sample buffer was exchanged for 100 mM KCl, 0.05% DDM, pH adjusted to ~8 with 50 mM KOH using gel filtration on a pre-packed Sephadex G-25 column (PD-10; Pharmacia). The pH during measurement was found to be 7.5–7.7. Traces were collected also in the presence of buffer (100 mM HEPES-NaOH at pH 7.5, 0.05% DDM) and they were subtracted from those obtained in the buffer-free solution in order to remove possible contribution of the hemes (about 12 traces were averaged). To estimate the number of protons taken up per enzyme molecule, the exhaust solution from the stopped-flow apparatus (in the absence of buffer) was collected, its pH was adjusted to 8.0 and absorbance changes corresponding to a given proton concentration were determined by additions of well-defined amounts of hydrochloric acid.

Determination of the heme concentration

The concentration of heme *b* was determined from the absorbance spectrum of the reduced ba_3 Cyt*c*O using the absorption coefficient ε(560–590) = 26 $mM^{-1}cm^{-1}$ (28) or from a

reduced *minus* oxidized spectrum with ε(560–658) = 21 $mM^{-1}cm^{-1}$. Ferro-heme a_{s3} was quantified using ε(613–658) = 6.3 $mM^{-1}cm^{-1}$ in the reduced *minus* oxidized spectrum (32).

Results

Four-electron reduced enzyme

A solution of the fully reduced ba_3 Cyt*c*O with CO bound to heme a_3 was mixed with an oxygen-saturated solution after which the CO ligand was dissociated by means of a laser flash approximately 30 ms after mixing. Upon removal of the CO ligand, O_2 binds to heme a_3, which initiates the reaction. Figure 2ab shows absorbance changes at 560 nm and 610 nm for the T312V and Y244F mutant Cyt*c*Os, compared to those obtained with the wild-type Cyt*c*Os. The rate constants are summarized in Table 1. At 560 nm the absorbance changes are dominated by heme *b*. With the wild-type Cyt*c*O, after flash-photolysis of CO at *t*=0, a decrease in absorbance is seen (Figure 2a), which is associated with oxidation of heme *b* upon electron transfer to the catalytic site forming intermediate $\mathbf{P_R}$ with a rate constant of $6.8{\cdot}10^4$ s^{-1} (τ≈15 μs). In the T312V and Y244F mutant Cyt*c*Os this reaction rate was about the same, ~$6.6{\cdot}10^4$ s^{-1} (τ≈15 μs) or slightly slower ~$4.4{\cdot}10^4$ s^{-1} (τ≈22 μs), respectively. The same process is also seen at 610 nm where the $\mathbf{P_R}$ state displays maximum absorbance (Figure 2b) (see comment in Table 1).

The subsequent increase in absorbance at 560 nm (re-reduction of heme *b*) occurs upon electron transfer from Cu_A to heme *b*, which is also seen as an absorbance increase at 830 nm, attributed to oxidation of Cu_A (not shown). This reaction displayed rate constants of ~$1.3{\times}10^4$ s^{-1} (τ≈80 μs) and ~$0.85{\times}10^4$ s^{-1} (τ≈120 μs) for the T312V and Y244F mutant ba_3 Cyt*c*Os, respectively (Figure 2a) being slightly slower than with the wild-type Cyt*c*O (~$1.6{\times}10^4$ s^{-1}, τ≈60 μs). With the wild-type Cyt*c*O this electron transfer is also linked in time to proton uptake from solution ($1.4–1.7{\times}10^4$ s^{-1} (τ≈60–70 μs), as measured by monitoring absorbance changes of a pH-sensitive dye, cresol red at 575 nm (Figure 3). With the T312V and Y244F mutant Cyt*c*Os the proton uptake was slowed by approximately a factor of two to 0.83×10^4 s^{-1} (τ≈120 μs) and 0.76×10^4 s^{-1} (τ≈130 μs), respectively. With the wild-type Cyt*c*O this proton is presumably transferred to a protonloading site (PLS) that is located at a distance from the catalytic site (see Discussion).

The decrease in absorbance at 610 nm with a rate constant of ~$1.3{\times}10^3$ s^{-1} (τ≈0.8 ms) with the wild-type Cyt*c*O is associated with decay of the $\mathbf{P_R}$ state and presumably formation of the **F** state. This decrease displayed about the same rate constants with the T312V and Y244F mutant Cyt*c*Os, $1.2{\cdot}10^3$ s^{-1} (τ≈0.8 ms) and $0.9{\cdot}10^3$ s^{-1} (τ≈1.1 ms), respectively (Figure 2b, Table 1).

The final decrease in absorbance at 560 nm, associated with formation of the oxidized state displayed a rate constant of 900 s^{-1} (τ≈1.1 ms) with the wild-type Cyt*c*O. At neutral pH this absorbance decrease occurs approximately with the same rate as the slower proton uptake (~$1.1{\times}10^3$ s^{-1}, τ≈0.9 ms) and the decrease in absorbance at 610 nm (~$1.3{\times}10^3$ s^{-1}, τ≈0.8 ms), associated with decay of the $\mathbf{P_R}$ state (Table 1). However, at higher pH values the 560 nm decrease in absorbance (oxidation of the Cyt*c*O) is significantly slowed. This reaction occurs after the decay at 610 nm ($\mathbf{P_R}$ decay), accompanied by simultaneous proton uptake,

where the two latter are essentially unaffected by an elevated pH. In other words, the 560 nm and 610 nm absorbance changes represent processes that at neutral pH by coincidence display approximately the same rate constants, while at high pH, only the $\mathbf{P_R}$ decay (610 nm) and proton uptake remain linked in time (21–23). With the T312V and Y244F mutant Cyt*c*Os the oxidation of the Cyt*c*O and proton uptake were significantly slowed to ~170 s^{-1} ($\tau\approx$5.8 ms) and 190 s^{-1} (5.2 ms) for the two mutant Cyt*c*Os, respectively (Figure 3), and occurred after the 610-nm absorbance decrease (0.8 ms and 1.1 ms, respectively). In other words, in contrast to the wild-type Cyt*c*O, with both mutant Cyt*c*Os the final oxidation of the Cyt*c*O (absorbance decrease at 560 nm) was accompanied by (a slowed) proton uptake with the same time constant as the oxidation process (Figures 2a and 3). We also note that in the mutant Cyt*c*Os formation of state **F** was not linked in time to proton uptake *from solution* even though the $\mathbf{P_R} \rightarrow \mathbf{F}$ reaction requires proton transfer to the catalytic site (see Discussion).

The amplitudes of the pH dye absorbance changes, associated with proton uptake, were recalculated into proton-concentration changes by titration of the buffer capacity of the sample (see “Materials and Methods”). The total stoichiometry of proton uptake was approximately 2 H^+ per Cyt*c*O for both the wild-type and mutant Cyt*c*Os, with approximately equal contributions of the two components.

Three-electron reduced enzyme

To monitor proton uptake that is required for (and triggered by) formation of the **F** state without interference from the next reaction step, we studied the reaction of the three-electron reduced Cyt*c*O with O_2 (Figure 2c–e) (22, 23). In this state Cu_A is oxidized and all other redox sites are reduced. As seen previously with the wild-type Cyt*c*O (22, 23), after O_2 binding to heme a_3 and the initial absorbance decrease at 560 nm (Figure 2c), associated with oxidation of heme *b*, no further absorbance changes were observed, i.e. heme *b* was not re-reduced because Cu_A was initially oxidized. This conclusion was confirmed by the absence of any absorbance changes at 830 nm (reflecting redox changes at Cu_A, Figure 2e). As with the wild-type Cyt*c*O, with the T312V and Y244F mutant Cyt*c*Os the rate constants of heme *b* oxidation were about a factor of two slower for the three-electron reduced Cyt*c*O compared to the four-electron reduced variant, 3.2×10^3 s^{-1} ($\tau\approx$30 μs) and 2.9×10^3 s^{-1} ($\tau\approx$34 μs), respectively. In this case these absorbance changes coincided in time with those observed at 610 nm (increase in absorbance), i.e. oxidation of heme *b* and formation of $\mathbf{P_R}$ occurred over the same time scales. Formation of the **F** state with the T312V and Y244F mutant Cyt*c*Os was observed as a decrease in absorbance at 610 nm with rate constants of 0.95×10^3 s^{-1} ($\tau\approx$1 ms) and 0.90×10^3 s^{-1} ($\tau\approx$1.1 ms), respectively (Figure 2d). Generally, the rates were very similar to those observed with the four-electron reduced enzyme.

The net proton uptake during reaction of the three-electron reduced Cyt*c*O with O_2 is shown in Figure 3. With the wild-type ba_3 Cyt*c*O, two components were observed with time constants of 70 μs and 1 ms, respectively, and the net stoichiometry was similar to that observed with the four-electron reduced Cyt*c*O (23). With the T312V and Y244F mutant Cyt*c*Os the rapid proton-uptake phase displayed rate constants of $0.83\cdot10^4$ s^{-1} ($\tau\approx$120 μs) and $0.67\cdot10^3$ s^{-1} (150 μs), respectively. This kinetic component displayed the same

amplitude and about the same rate as for the four-electron reduced Cyt*c*Os. The second proton-uptake component displayed significantly smaller amplitudes (~30%) than with the wild-type three-electron reduced Cyt*c*O, and for the T312V mutant Cyt*c*O the rate was slightly faster than that observed with the four-electron reduced Cyt*c*O (see Table 1).

Discussion

Results from recent studies of the ba_3 Cyt*c*O from *T. thermophilus* indicate that the reaction sequence is similar to that of the well-studied aa_3 Cyt*c*Os (20, 22). However, there are significant differences in the timing of the proton-transfer reactions as outlined in the Introduction. Briefly, in the wild-type ba_3 Cyt*c*O, first an electron is transferred from heme *b* to the catalytic site forming state $\mathbf{P_R}$ with a time constant of ~15 μs. Then, a proton is taken up from solution with a time constant of ~60 μs. However, in contrast to the aa_3 Cyt*c*O, the proton is not transferred to the catalytic site to form state **F**, but presumably to the PLS. Over a slower time scale the $\mathbf{P_R}$ state decays, accompanied by proton uptake to the catalytic site with a time constant of ~1 ms. With the wild-type Cyt*c*O, at neutral pH the decay of the $\mathbf{P_R}$ state occurs approximately at the same time as formation of the oxidized Cyt*c*O and therefore state **F** is not observed (22) (see also (20)). However, at high pH the two events, $\mathbf{P_R} \rightarrow \mathbf{F}$ and $\mathbf{F} \rightarrow \mathbf{O}$, are separated in time because the latter is significantly slower than the former.

In the wild-type ba_3 Cyt*c*O the last step, i.e., the $\mathbf{F} \rightarrow \mathbf{O}$ reaction is not accompanied by any *net* proton uptake when measured in solution. Because formation of the oxidized Cyt*c*O (state **O**) does require proton transfer to the catalytic site, we proposed that during the $\mathbf{F} \rightarrow \mathbf{O}$ reaction the proton residing at PLS is released simultaneously with proton uptake to the catalytic site. With the T312V and Y244F mutant Cyt*c*Os heme *b* was oxidized with the same time constant (T312V, $\tau \approxeq 15$ μs) or slightly slower (Y244F, $\tau \approxeq 22$ μs) than with the wild-type Cyt*c*O. The increase in absorbance at 560 nm (electron transfer from Cu_A to heme *b*) and the accompanying first proton uptake (to the PLS in the wild-type Cyt*c*O) were both slowed from ~60 μs to ~120–130 μs with the mutant Cyt*c*Os (Figures 2a and 3, Table 1), which is a relatively small effect. In the next step, the absorbance decrease at 610 nm displayed about the same time constant with the T312V and Y244F mutant Cyt*c*Os as with the wild-type Cyt*c*O, which indicates that the $\mathbf{P_R}$ state decayed (and presumably **F** was formed) with the same time constants of approximately 1.0 ms (Table 1).

The main differences in the reaction sequences of the wild-type and mutant Cyt*c*Os were observed at this point in time. While with the wild-type Cyt*c*O the absorbance decay at 610 nm coincides in time with proton uptake (c.f. Figures 2b and 3a), in the T312V and Y244F mutant Cyt*c*Os no net proton uptake was observed on this time scale (c.f. Figures 2b and 3bc), which is surprising given that formation of state **F** requires proton transfer to the catalytic site. The absence of any *net* proton uptake from solution could be explained by:

- **i.** release of the proton at PLS (taken up earlier, c.f. first proton uptake) to the *p* side over the same time scale as proton uptake to the catalytic site from the *n* side of the membrane (to form state **F**). This scenario would imply proton pumping over the same time scale as with the wild-type Cyt*c*O, but the proton release to the *p* side

would now be linked to formation of the **F** state rather than formation of the **O** state (as with the wildtype Cyt*c*O (Figure 1b)).

ii. internal transfer of the proton initially taken up to the PLS ($\tau \approx 120–130$ μs) from the PLS to the catalytic site (to form **F**) over a time scale of ~1 ms without any additional proton uptake from solution.

While the first scenario (*i*) is compatible with proton pumping, the second (*ii*) is not, at least during the reaction steps investigate here. The relatively active Y244F mutant Cyt*c*O (activity 15% of that of the wild-type Cyt*c*O) pumps protons (10), which is compatible with scenario (*i*) above. The very low activity of the T312V mutant Cyt*c*O (<1%) did not allow for a determination of the pumping stoichiometry (10). Such a low activity due to a mutation in the proton pathway suggests that at some point in the reaction cycle, proton transfer is dramatically slowed, which most likely would reduce the pumping stoichiometry (27, 33) because there would be sufficient time for the proton at PLS to be transferred to the catalytic site. In this case scenario (*ii*) would explain the behavior of the T312V mutant Cyt*c*O (see Figure 1b).

As already noted above, with the wild-type ba_3 Cyt*c*O there is no net proton uptake during the final step of oxidation of heme *b* and formation of the oxidized (**O**) enzyme. This observation was previously explained in terms of proton uptake from the *n* side to the catalytic site that coincides in time with release of a proton to the *p* side from the PLS (22). In contrast, the behavior of the T312V and Y244F mutant Cyt*c*Os was different in that we did observe proton uptake over the time scale of **O** formation ($\tau \approx 5–6$ ms), but, as outlined above, in these mutant Cyt*c*Os there was no net proton uptake upon **F** formation. Taken together, these two observations indicate that the PLS in the two mutant enzymes is not protonated in state **F**. A net proton uptake is observed during the $\mathbf{F} \rightarrow \mathbf{O}$ reaction because this reaction does not coincide with proton release from PLS (as it does with the wild-type Cyt*c*O).

The sequence of events in the variants were further investigated using the threeelectron reduced Cyt*c*O (Figure 2c–e) in which the reaction with O_2 stops upon forming the **F** state. With the wild-type ba_3 Cyt*c*O this reaction is accompanied by proton uptake with time constants of ~70 μs and 1 ms, where the first proton has been suggested to be transferred to the PLS and the second to the catalytic site to form the end product, state **F** (22, 23). With the T312V and Y244F mutant Cyt*c*Os only the first proton uptake displayed about the same rate and amplitude as observed with the wild-type Cyt*c*O, while the second proton-uptake phase displayed a significantly smaller amplitude (30 % of that observed with the four-electron reduced Cyt*c*O) (Figure 3bc). These observations are consistent with the explanation above, i.e., that, in the major fraction of the mutant enzyme population, the proton needed to form state **F** is either taken internally from within the Cyt*c*O (scenario *ii*), or it is accompanied by simultaneous proton release to the *p* side (scenario *i*).

The identity of the PLS, which is assumed to be the same for all heme-copper oxidases, is so far not known. Nevertheless, the number of candidates is limited (4, 34). For the ba_3 Cyt*c*O there is data suggesting that propionate A of heme a_3, possibly together with nearby sites at a hydrogen-bonding distance, may be involved in proton gating (8, 10, 34–36), see also (4,

37). For example, data from studies of CO photolysis from heme a_3 suggest that changes in the ligation state at the catalytic may be linked to changes in structure and protonation state of residues near the heme a_3 propionate A (35, 38).

In the ba_3 oxidase both substrate and pumped protons are transferred through a single pathway. The data suggests that transfer of the first proton to the PLS is faster than that to the catalytic site. In the wild-type Cyt*c*O, after protonation of PLS, the proton to the catalytic site must be transferred from solution and not from the PLS in order to allow pumping. One possibility to regulate the proton flow is by means of a local structural change (e.g. relocation of a side chain) that would allow alternating access to the PLS and the catalytic site respectively. In addition, proton transfer to and from the PLS must be controlled such that the PLS is protonated only from the *n*-side and deprotonated only to the *p*-side.

Structural modeling of the K-pathway analog of the ba_3 oxidase indicates that a water molecule is hydrogen bonded to Thr312 and interacts with Tyr244 (10). The Y244F mutation must not necessarily destabilize this water molecule, but in the T312V mutant Cyt*c*O it is likely to be lost. Yet, the data from this study suggest that the effect of the T312V and Y244F mutations is not to significantly modify the proton conductivity of the pathway because the rate of the first proton uptake was only a factor of two slower than that of the wild-type Cyt*c*O. Yet, proton uptake that followed in time after this first proton uptake was slower with both mutant Cyt*c*Os. This observation suggests that the effect of the mutations is not to slow proton transfer *per se* (c.f. the rate of the first proton uptake was not significantly affected). We speculate that the mutations instead interfere with structural changes that follow in time after the initial proton transfer to the PLS and that these changes are rate limiting for the second proton transfer. These structural changes are suggested to involve a segment of the proton pathway “below” the catalytic site because residues T312 and Y244 are located in this segment (Figure 1a). The structural modifications at these sites are suggested to control proton transfer to the catalytic site and the PLS, respectively. In addition, these changes would have to involve also a segment of the protein around the PLS to control proton transfer to and from this site. A link between structural changes below and above the hemes during turnover is expected because the enzyme must control the proton flux to the catalytic site and to/from the PLS. A comparable scenario has been observed, for example, with the *R. sphaeroides* aa_3 Cyt*c*O where the flux of protons to the catalytic site and the PLS, respectively, is presumably controlled by Glu286. Any structural changes at Glu286, “below” the catalytic site would be linked to changes at a putative PLS, located “above” the hemes. Furthermore, proton pumping has been shown to be uncoupled from O_2 reduction upon mutation of residues close the *n*-side surface of the Cyt*c*O, i.e. at a significant distance from Glu286 (33, 39–42).

The modulation of the structural changes by the T312V and Y244F mutations would result in slowed uptake of the *second* proton to form state **F** such that in the mutant Cyt*c*O this proton uptake occurs over the same time scale as proton release to the *p* side (scenario *i* above for the Y244F). Alternatively, a mutation that interferes with the structural changes may lead to slowed release of the proton from PLS, such that the proton is transferred back to the catalytic site as outlined in case *ii* above (possibly for the T312V mutant Cyt*c*O). It

should be mentioned that observation of proton pumping without a membrane potential (or with a small potential present) as is the case in standard pumping measurements, does not directly imply that proton pumping also takes place in the presence of a transmembrane proton electrochemical gradient. It is possible that any structural changes that lead to alteration in the temporal sequence of the proton pump, may reveal their full effect only in the presence of a transmembrane potential (i.e. the Y244F mutant Cyt*c*O may display a lower pumping stoichiometry *in vivo*).

Taken together, although the key structural elements (e.g. the PLS, catalytic site) are the same in the wild-type and mutant Cyt*c*Os, the structural changes required to control the access to these sites might be perturbed, which would result in uncontrolled release either to the *p* side or proton transfer from the PLS to the catalytic site. For the T312V mutant Cyt*c*O, this conclusion is further supported by the differences in effects of the mutation observed for the Cyt*c*O turnover (<3e^-/s and for oxidation of the mutant Cyt*c*O where the slowest component displayed a time constant of ~6 ms (because during oxidation of the Cyt*c*O four electrons are transferred to O_2, the time constant for transfer of one electron is 6 ms/4 = 1.5 ms, i.e. the corresponding turnover rate would be ~670 electrons·s^{-1}, i.e. a factor of >200 faster than the actual turnover rate). Apparently, there must be rate-limiting events, which take place during turnover, but not during oxidation of the reduced Cyt*c*O (c.f. the structural changes controlling the proton pump). In an earlier study, we investigated the reaction of reduced T315V and T312S mutant Cyt*c*Os with O_2 (24). At the time of that study, the sequence of proton-transfer events in the wild-type ba_3 Cyt*c*O was not well understood. Now, we can offer more reliable mechanistic speculations in the framework of more recent data, including those from the present study. The residue Thr315 is located about 5 Å below Thr312 in the K-pathway analog. In the case of the T315V Cyt*c*O the pumping stoichiometry could be measured (the activity was 6 % of that of the wild-type Cyt*c*O) (10) and the mutant Cyt*c*O was found not to pump protons. Qualitatively, the T315V mutant Cyt*c*O displayed the same behavior as the T312V mutant Cyt*c*O (see Table 1) studied here (c.f. scenario *ii*), i.e. the 610 nm absorbance decrease occurred before final oxidation of the Cyt*c*O without any accompanying proton uptake from solution.

With the T312S mutant Cyt*c*O, which pumps protons (the activity was 13 % of that of the wild-type Cyt*c*O) the formation of state $\mathbf{P_R}$ and proton transfer to PLS were only slightly slowed (by less than a factor of 3), while uptake of the second proton was slowed dramatically to ~25 s^{-1} (24). However, in contrast to the results with the T312V mutant Cyt*c*O from the present work, with the T312S mutant Cyt*c*O state **F** was not observed. Instead the 610 nm absorbance decayed approximately over the same time scale as oxidation of the Cyt*c*O (see Table 1). We conclude that with the T312S mutant Cyt*c*O (back)proton transfer from PLS to the catalytic site could not take place and the PLS remained protonated (similar to the scenario observed with the Y244F mutant Cyt*c*O, scenario (*i*) above). In order to form the fully oxidized Cyt*c*O a net of two protons must be taken up to the catalytic site. However, after the initial proton transfer to PLS in the T312S mutant Cyt*c*O a net uptake of only one proton was observed over the time scale of oxidation of the Cyt*c*O, which would suggest that formation of the oxidized Cyt*c*O was accompanied by release of the PLS proton, i.e. proton pumping. Again, these earlier data support the model discussed above

because the T312S mutant Cyt*c*O was found to pump protons (10). Also, the turnover rate for the T312S mutant Cyt*c*O (~40 s^{-1}) is only a factor of 2.5 slower than the oxidation rate (for the T312V mutant Cyt*c*O the difference was a factor of >200, as outlined above) because with this mutant Cyt*c*O the slowest component displayed a rate constant of 25 s^{-1} (for four electrons, see above) i.e. corresponding to a turnover rate of ~100 electrons/s.

In summary, the results from the present study indicate that proton transfer to the catalytic site and the PLS of the ba_3 Cyt*c*O can be modulated independently of each other by means of site-directed structural modifications of residues Y244 and T312 within the K proton pathway analog. Furthermore, the data suggest that in the wild-type Cyt*c*O proton transfer through this proton pathway to the PLS and the catalytic site is controlled by means of structural rearrangements that involve residues Y244 and T312.

Acknowledgments

Funding: These studies were supported by grants from the Swedish Research Council and by grant HL 16101 from the National Institutes of Health. IS was supported by a grant from Stockholm University.

Abbreviations

Cyt*c*O	cytochrome *c* oxidase
***n* side**	negative side of the membrane
***p* side**	positive side of the membrane
R	the four-electron reduced Cyt*c*O
A	reduced Cyt*c*O with O_2 bound to heme a_3
P_R	the “peroxy” state formed after transfer of a third electron to the catalytic site
F	the ferryl state formed at the catalytic site after protonation of P_R
O	the oxidized Cyt*c*O
DDM	n-Dodecyl β-D-maltoside

References

1. Hosler JP, Ferguson-Miller S, Mills DA. Energy transduction: Proton transfer through the respiratory complexes. Annual Review of Biochemistry. 2006; 75:165–187.
2. Belevich I, Verkhovsky MI. Molecular mechanism of proton translocation by cytochrome c oxidase. Antioxid Redox Signal. 2008; 10:1–29. [PubMed: 17949262]
3. Ferguson-Miller S, Babcock GT. Heme/copper terminal oxidases. Chem Rev. 1996; 96:2889–2907. [PubMed: 11848844]
4. Wikström M, Verkhovsky MI. Mechanism and energetics of proton translocation by the respiratory heme-copper oxidases. Biochimica et Biophysica Acta (BBA) - Bioenergetics. 2007; 1767:1200–1214.
5. Brzezinski P, Gennis RB. Cytochrome c oxidase: exciting progress and remaining mysteries. J Bioenerg Biomembr. 2008; 40:521–531. [PubMed: 18975062]
6. Soulimane T, Than ME, Dewor M, Huber R, Buse G. Primary structure of a novel subunit in ba3-cytochrome oxidase from Thermus thermophilus. Protein Science. 2000; 9:2068–2073. [PubMed: 11152118]

7. Tiefenbrunn T, Liu W, Chen Y, Katritch V, Stout CD, Fee JA, Cherezov V. High resolution structure of the ba3 cytochrome c oxidase from thermus thermophilus in a lipidic environment. PLoS ONE. 2011; 6
8. Soulimane T, Buse G, Bourenkov GP, Bartunik HD, Huber R, Than ME. Structure and mechanism of the aberrant ba_3-cytochrome *c* oxidase from *Thermus thermophilus*. EMBO J. 2000; 19:1766–1776. [PubMed: 10775261]
9. Luna VM, Chen Y, Fee JA, Stout CD. Crystallographic studies of Xe and Kr binding within the large internal cavity of cytochrome ba_3 from Thermus thermophilus: Structural analysis and role of oxygen transport channels in the heme-Cu oxidases. Biochemistry. 2008; 47:4657–4665. [PubMed: 18376849]
10. Chang HY, Hemp J, Chen Y, Fee JA, Gennis RB. The cytochrome ba3 oxygen reductase from Thermus thermophilus uses a single input channel for proton delivery to the active site and for proton pumping. Proc Natl Acad Sci U S A. 2009; 106:16169–16173. [PubMed: 19805275]
11. Iwata S, Ostermeier C, Ludwig B, Michel H. Structure at 2.8 Å resolution of cytochrome c oxidase from Paracoccus denitrificans. Nature. 1995; 376:660–669. [PubMed: 7651515]
12. Svensson-Ek M, Abramson J, Larsson G, Törnroth S, Brzezinski P, Iwata S. The X-ray Crystal Structures of Wild-Type and EQ(I-286) Mutant Cytochrome *c* Oxidases from *Rhodobacter sphaeroides*. J Mol Biol. 2002; 321:329–339. [PubMed: 12144789]
13. Tsukihara T, Aoyama H, Yamashita E, Tomizaki T, Yamaguchi H, Shinzawa-Itoh K, Nakashima R, Yaono R, Yoshikawa S. The whole structure of the 13-subunit oxidized cytochrome c oxidase at 2.8 Å. Science. 1996; 272:1136–1144. [PubMed: 8638158]
14. Liu J, Qin L, Ferguson-Miller S. Crystallographic and online spectral evidence for role of conformational change and conserved water in cytochrome oxidase proton pump. Proc Natl Acad Sci U S A. 2011; 108:1284–1289. [PubMed: 21205904]
15. Qin L, Hiser C, Mulichak A, Garavito RM, Ferguson-Miller S. Identification of conserved lipid/detergent-binding sites in a high-resolution structure of the membrane protein cytochrome c oxidase. Proc Natl Acad Sci U S A. 2006; 103:16117–16122. [PubMed: 17050688]
16. Shinzawa-Itoh K, Aoyama H, Muramoto K, Terada H, Kurauchi T, Tadehara Y, Yamasaki A, Sugimura T, Kurono S, Tsujimoto K, Mizushima T, Yamashita E, Tsukihara T, Yoshikawa S. Structures and physiological roles of 13 integral lipids of bovine heart cytochrome c oxidase. EMBO Journal. 2007; 26:1713–1725. [PubMed: 17332748]
17. Aoyama H, Muramoto K, Shinzawa-Itoh K, Hirata K, Yamashita E, Tsukihara T, Ogura T, Yoshikawa S. A peroxide bridge between Fe and Cu ions in the O2 reduction site of fully oxidized cytochrome c oxidase could suppress the proton pump. Proc Natl Acad Sci U S A. 2009; 106:2165–2169. [PubMed: 19164527]
18. Radzi Noor M, Soulimane T. Bioenergetics at extreme temperature: Thermus thermophilus ba 3- and caa 3-type cytochrome c oxidases. Biochimica et Biophysica Acta - Bioenergetics. 2012; 1817:638–649.
19. Hemp J, Gennis RB. Diversity of the heme-copper superfamily in archaea: insights from genomics and structural modeling. Results Probl Cell Differ. 2008; 45:1–31. [PubMed: 18183358]
20. Siletsky SA, Belevich I, Jasaitis A, Konstantinov AA, Wikström M, Soulimane T, Verkhovsky MI. Time-resolved single-turnover of ba3 oxidase from Thermus thermophilus. Biochim Biophys Acta. 2007; 1767:1383–1392. [PubMed: 17964277]
21. Von Ballmoos C, Lachmann P, Gennis RB, Ädelroth P, Brzezinski P. Timing of electron and proton transfer in the ba 3 cytochrome c oxidase from Thermus thermophilus. Biochemistry. 2012; 51:4507–4517. [PubMed: 22624600]
22. Von Ballmoos C, Ädelroth P, Gennis RB, Brzezinski P. Proton transfer in ba_3 cytochrome c oxidase from *Thermus thermophilus*. Biochimica et Biophysica Acta - Bioenergetics. 2012; 1817:650–657.
23. Von Ballmoos C, Gennis RB, Ädelroth P, Brzezinski P. Kinetic design of the respiratory oxidases. Proc Natl Acad Sci U S A. 2011; 108:11057–11062. [PubMed: 21690359]
24. Smirnova I, Reimann J, Von Ballmoos C, Chang HY, Gennis RB, Fee JA, Brzezinski P, Ädelroth P. Functional role of Thr-312 and Thr-315 in the proton-transfer pathway in ba_3 cytochrome *c* oxidase from thermus thermophilus. Biochemistry. 2010; 49:7033–7039. [PubMed: 20677778]

25. Kannt A, Soulimane T, Buse G, Becker A, Bamberg E, Michel H. Electrical current generation and proton pumping catalyzed by the ba3- type cytochrome c oxidase from Thermus thermophilus. FEBS Lett. 1998; 434:17–22. [PubMed: 9738443]
26. Han H, Hemp J, Pace LA, Ouyang H, Ganesan K, Roh JH, Daldal F, Blanke SR, Gennis RB. Adaptation of aerobic respiration to low O2 environments. Proceedings of the National Academy of Sciences. 2011; 108:14109–14114.
27. Namslauer A, Brzezinski P. Structural elements involved in electron-coupled proton transfer in cytochrome c oxidase. FEBS Lett. 2004; 567:103–110. [PubMed: 15165901]
28. Chen Y, Hunsicker-Wang L, Pacoma RL, Luna E, Fee JA. A homologous expression system for obtaining engineered cytochrome ba 3 from Thermus thermophilus HB8. Protein Expr Purif. 2005; 40:299–318. [PubMed: 15766872]
29. Ädelroth P, Ek M, Brzezinski P. Factors Determining Electron-Transfer Rates in Cytochrome *c* Oxidase: Investigation of the Oxygen Reaction in the *R. sphaeroid*es and Bovine Enzymes. Biochim Biophys Acta. 1998; 1367:107–117. [PubMed: 9784618]
30. Ädelroth P, Svensson-Ek M, Mitchell DM, Gennis RB, Brzezinski P. Glutamate 286 in cytochrome aa3 from Rhodobacter sphaeroides is involved in proton uptake during the reaction of the fully-reduced enzyme with dioxygen. Biochemistry. 1997; 36:13824–13829. [PubMed: 9374859]
31. Brändén M, Sigurdson H, Namslauer A, Gennis RB, Ädelroth P, Brzezinski P. On the role of the K-proton transfer pathway in cytochrome c oxidase. Proc Natl Acad Sci U S A. 2001; 98:5013–5018. [PubMed: 11296255]
32. Zimmermann BH, Nitsche CI, Fee JA, Rusnak F, Munck E. Properties of a copper-containing cytochrome ba3: a second terminal oxidase from the extreme thermophile Thermus thermophilus. Proc Natl Acad Sci U S A. 1988; 85:5779–5783. [PubMed: 2842747]
33. Brzezinski P, Johansson AL. Variable proton-pumping stoichiometry in structural variants of cytochrome c oxidase. Biochimica et Biophysica Acta - Bioenergetics. 2010; 1797:710–723.
34. Chang HY, Choi SK, Vakkasoglu AS, Chen Y, Hemp J, Fee JA, Gennis RB. Exploring the proton pump and exit pathway for pumped protons in cytochrome ba 3 from Thermus thermophilus. Proc Natl Acad Sci U S A. 2012; 109:5259–5264. [PubMed: 22431640]
35. Koutsoupakis C, Soulimane T, Varotsis C. Probing the Q-Proton Pathway of ba3-Cytochrome c Oxidase by Time-Resolved Fourier Transform Infrared Spectroscopy. Biophys J. 2004; 86:2438–2444. [PubMed: 15041681]
36. Fee JA, Case DA, Noodleman L. Toward a chemical mechanism of proton pumping by the B-type cytochrome c oxidases: Application of density functional theory to cytochrome ba_3 of Thermus thermophilus. J Am Chem Soc. 2008; 130:15002–15021. [PubMed: 18928258]
37. Kaila VRI, Sharma V, Wikström M. The identity of the transient proton loading site of the proton-pumping mechanism of cytochrome c oxidase. Biochimica et Biophysica Acta - Bioenergetics. 2011; 1807:80–84.
38. Koutsoupakis C, Soulimane T, Varotsis C. Ligand Binding in a Docking Site of Cytochrome c Oxidase: A Time-Resolved Step-Scan Fourier Transform Infrared Study. J Am Chem Soc. 2003; 125:14728–14732. [PubMed: 14640647]
39. Pfitzner U, Hoffmeier K, Harrenga A, Kannt A, Michel H, Bamberg E, Richter OMH, Ludwig B. Tracing the D-pathway in reconstituted sitedirected mutants of cytochrome c oxidase from Paracoccus denitrificans. Biochemistry. 2000; 39:6756–6762. [PubMed: 10841754]
40. Zhu J, Han H, Pawate A, Gennis RB. Decoupling mutations in the D-Channel of the aa_3-Type cytochrome *c* oxidase from *Rhodobacter sphaeroides* suggest that a continuous hydrogen-bonded chain of waters is essential for proton pumping. Biochemistry. 2010; 49:4476–4482. [PubMed: 20441187]
41. Johansson AL, Carlsson J, Högbom M, Hosler JP, Gennis RB, Brzezinski P. Proton uptake and pKa changes in the uncoupled Asn139Cys variant of cytochrome c oxidase. Biochemistry. 2013; 52:827–836. [PubMed: 23305515]
42. Johansson AL, Högbom M, Carlsson J, Gennis RB, Brzezinski P. Role of aspartate 132 at the orifice of a proton pathway in cytochrome c oxidase. Proc Natl Acad Sci U S A. 2013; 110:8912–8917. [PubMed: 23674679]

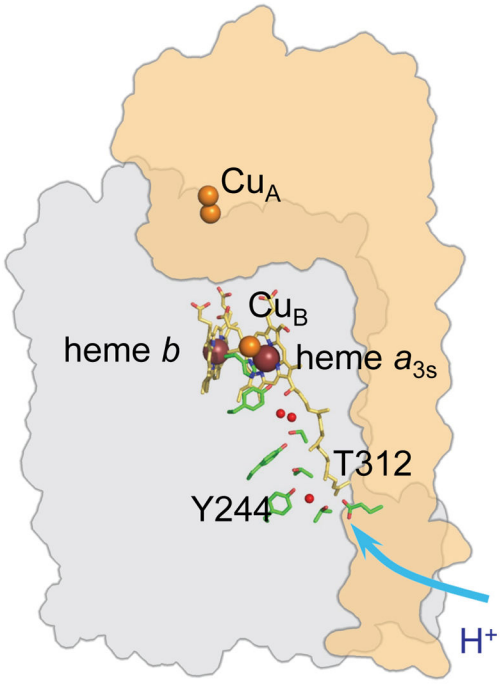

Fig 1a

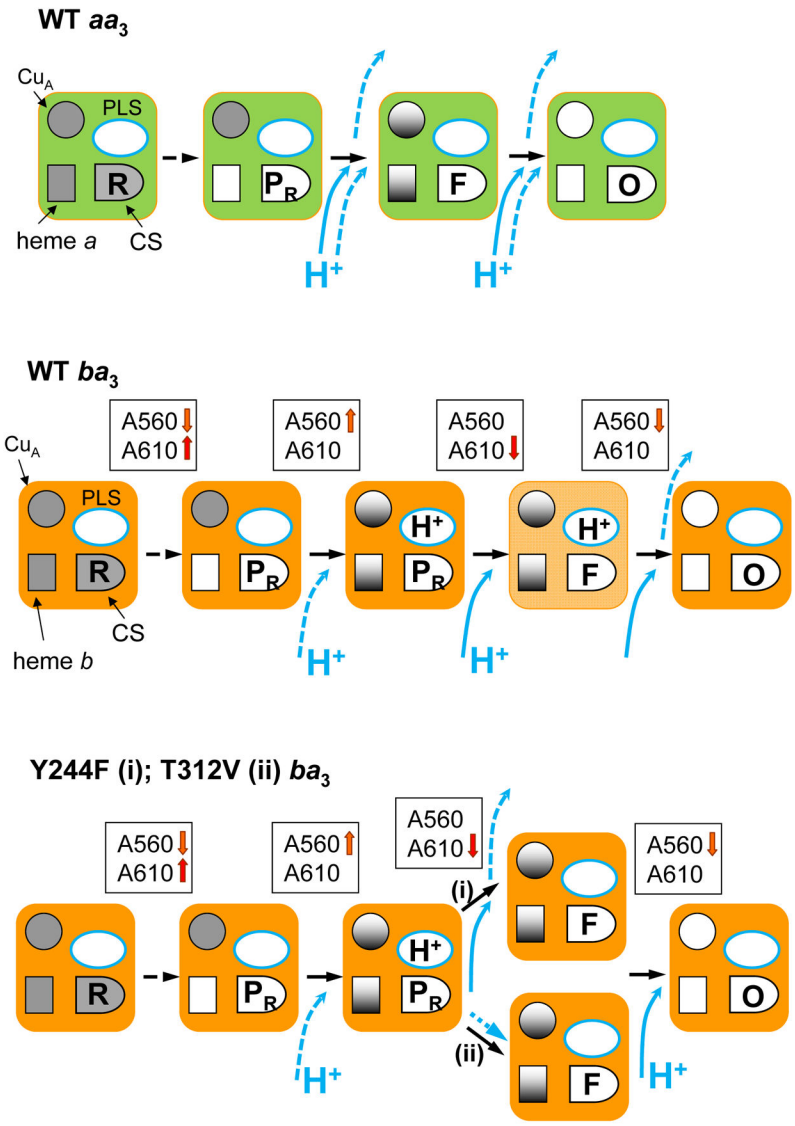

Fig 1b

Figure 1. Proton pathway and reaction scheme

(a) Residues that comprise the K-pathway analog used for transfer of both substrate protons to the catalytic site (used for O_2 reduction) and protons that are pumped across the membrane (Protein Data Bank: PDB3S8F (7). Copper and iron ions are presented as brown and orange spheres, respectively. Heme carbon atoms are shown in yellow and residues of the proton pathway are shown in green with oxygen and nitrogen atoms in red and blue, respectively. Water molecules of the proton-conducting pathway are shown as small red spheres.

(b) Schematic outline of the reaction of the four-electron reduced aa_3 and ba_3 Cyt*c*Os with O_2. The redox centers are shown as a circle (Cu_A), a square (heme *b* or *a* for the ba_3 and aa_3

oxidases, respectively) and a merged square-circle (catalytic site, CS), where filled and empty symbols represent reduced and oxidized centers, respectively. A putative “proton-loading site” (PLS) is shown just above the catalytic site. For the ba_3 Cyt*c*O the sign of absorbance changes (arrow up - increase in absorbance; arrow down, decrease in absorbance) of the different steps of the reaction are indicated in the square boxes. Protons that are pumped and transferred to the catalytic site are shown as dashed and solid lines, respectively. For the two mutant Cyt*c*Os, Y244F and T312V, two alternative scenarios (*i*) and (*ii*) are shown in the branched part of the lower reaction scheme. In scenario (*ii*) proton pumping does not occur because the proton at PLS is transferred to the catalytic site. This is illustrated by the blue dashed arrow next to (*ii*) in the third step of the lowermost scheme.

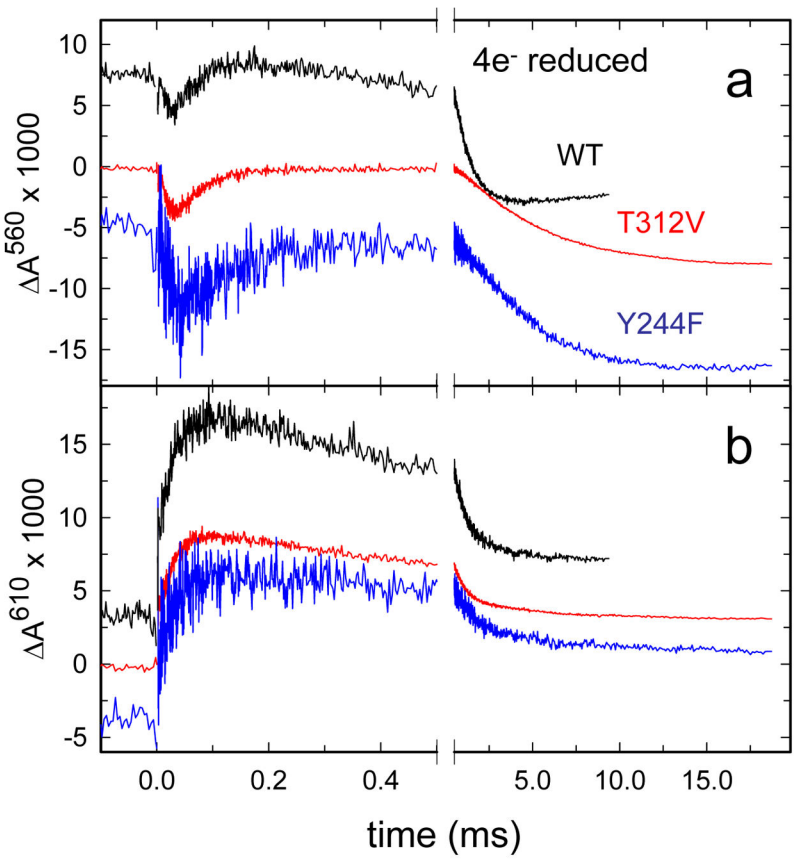

Fig. 2ab

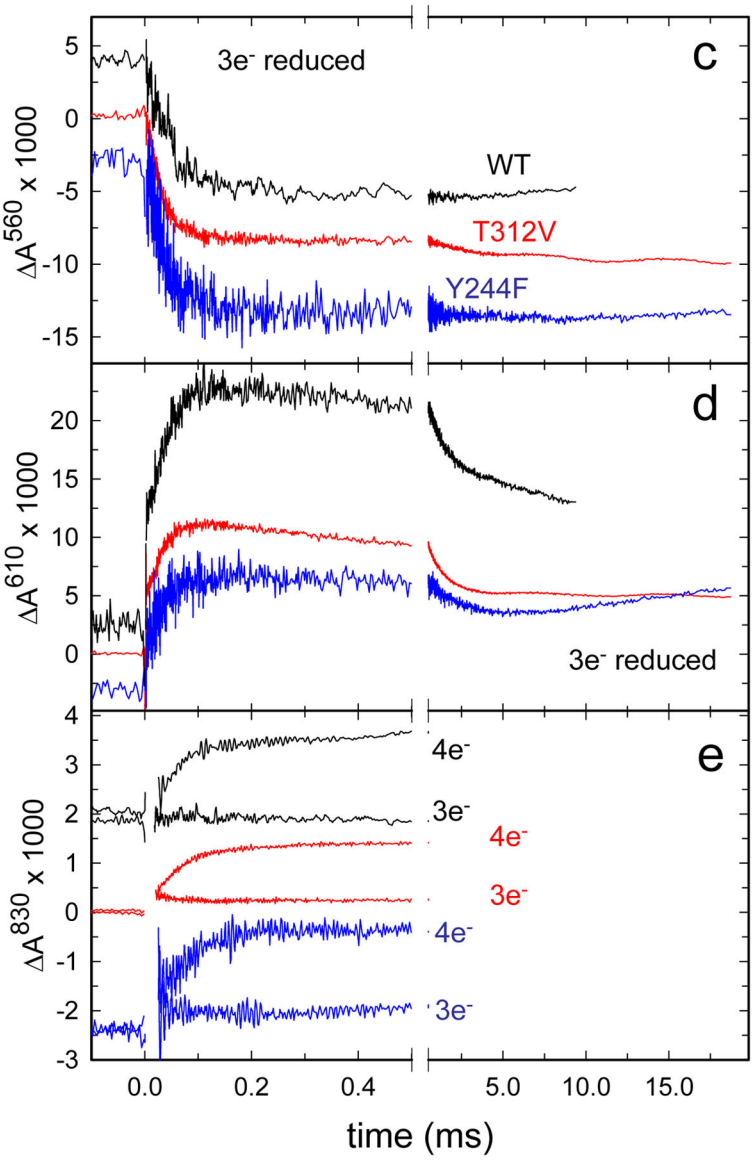

Fig. 2c-e

Figure 2. Absorbance changes associated with reaction of the reduced wild-type, T312V and Y244F mutant *ba*$_3$ oxidases withO_2

(**a,b**) Fully reduced Cyt*c*O (with four electrons) and (**c–e**) three-electron reduced Cyt*c*O. Absorbance changes are shown at 560 nm (**a** and **c**, main contribution from heme *b*), 610 nm (**b** and **d**, formation and decay of $\mathbf{P_R}$) and 830 nm (**e**, main contribution from Cu_A). In **e** traces are shown also for the 4-electron reduced Cyt*c*O for comparison. Traces plotted in black, red and blue correspond to wild-type, T312V and Y244F Cyt*c*Os, respectively. All trace were normalized to 1 μM reactive enzyme. Conditions: 100 mM HEPES-NaOH (pH 7.5), 0.05% DDM. The O_2 concentration was 1 mM after mixing. The reaction was initiated by a laser flash at t=0.

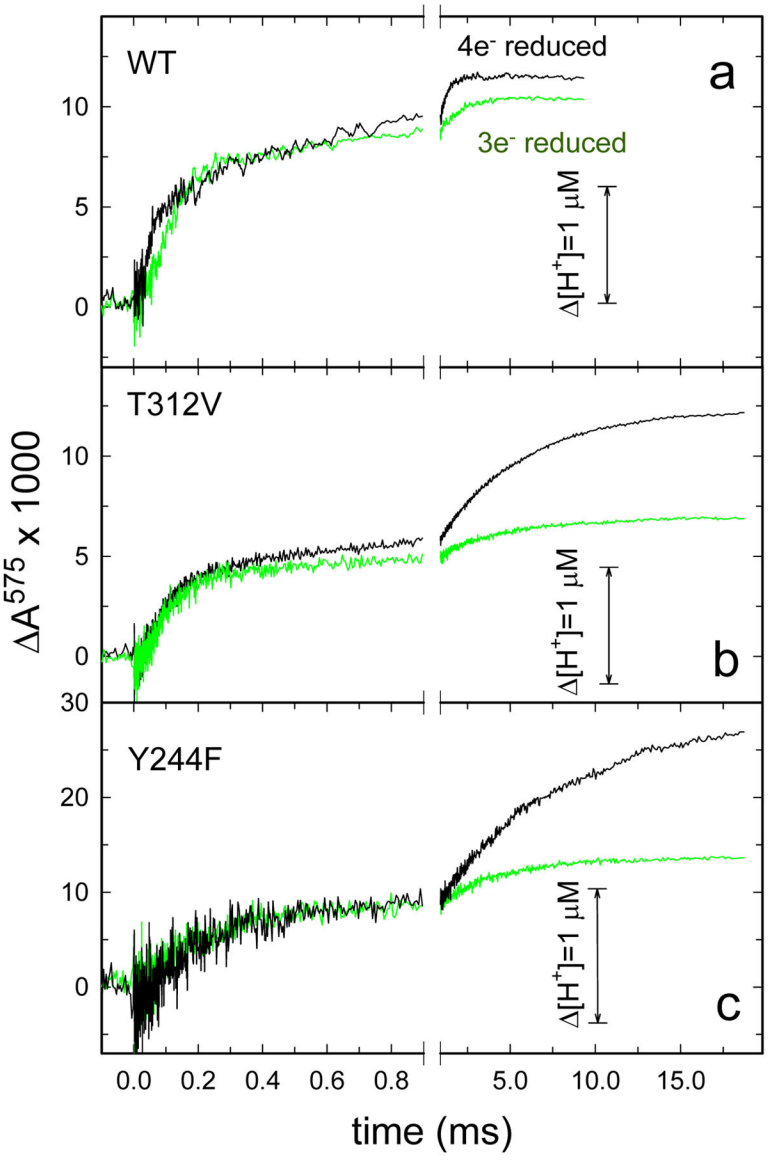

Fig. 3a-c

Figure 3. Absorbance changes associated with proton uptake

Proton uptake was followed as a function of time during reaction with O_2 of the four (black) and tree-electron (green) reduced wild-type (**a**), T312V (**b**) and Y244F (**c**) ba_3 CytcO. Measurements were done at 575 nm with 33 μM cresol red (after mixing). The traces are differences between those measured in unbuffered and buffered solutions. The reaction solutions contained 100 mM KCl (pH 7.5) (unbuffered solution) or 100 mM HEPES-NaOH (pH 7.5) (buffered solution), 0.05% DDM. Trace amplitudes were normalized to 1 μM reactive enzyme (see Methods).

Table 1

Rate constants of the absorbance changes during reaction of reduced wild-type and, T312V and Y244F mutant Cyt*c*Os with O_2 (pH 7.5). 4e and 3e refer to the four and three-electron reduced Cyt*c*Os, respectively. Rate constants were typically determined from at least four experiments. The standard error of the mean was ≤10%. pT, proton transfer; eT, electron transfer.

Observed absorbance changes	**ΔA560 decrease ΔA610 increase[#] (s^{-1})**	**ΔA560; ΔA830 increase (s^{-1})**	**1st proton uptake (s^{-1})**	**ΔA610 decrease (s^{-1})**	**ΔA560 slow decrease (s^{-1})**	**2nd proton uptake (s^{-1})**
Reaction	*formation of state P*	*fractional eT from Cu_A to heme b*	*pT to PLS*	*formation of state F*	*final oxidation*	*see* Fig 1b
WT 4e[#]	68000 (15 μs)	16000 (62 μs)	17000 (60 μs)	1300 (0.8 ms)	900 (1.1 ms)	1100 (0.9 ms)
T312V 4e	66000 (15 μs)	13000 (80 μs)	8300 (120 μs)	1200 (0.8 ms)	170 (6 ms)	170 (6 ms)
Y244F 4e	44000 (22 μs)	8500 (120 μs)	7600 (130 μs)	900 (1.1 ms)	190 (5.3 ms)	190 (5.3 ms)
WT 3e	30000 (30 μs)	no[¤]	14000 (70 μs)	1000 (1 ms)	no	1000 (1 ms)
T312V 3e	32000 (30 μs)	no	8300 (120 μs)	950 (1.0 ms)	no	290 (3.4 ms) (30%)
Y244F 3e	29000 (34 μs)	no	6700 (150 μs)	900 (1.1 ms)	no	190 (5.3 ms) (30%)
T312S 4e[&]	33000 (30 μs)	6000 (170 μs)	6000 (170 μs)	30 (33 ms)	30 (33 ms)	25 (40 ms)
T315V 4e[&]	68000 (15 μs)	13000 (77 μs)	8500 (120 μs)	~1000 (~1 ms)	200 (5 ms)	200 (5 ms)

[#]For the four-electron reduced Cyt*c*O (the wild-type and both mutant Cyt*c*Os) the absorbance decrease at 560 nm (oxidation of heme *b*) was about a factor of two faster than the increase in absorbance at 610 nm (formation of $\mathbf{P_R}$). This is a relatively small dissimilarity in rates and a detailed discussion of any functional differences would require more detailed studies, which is outside of the scope of the present manuscript. As done previously (21) we consider these two events to be synchronous until further studies are done.

[¤]no - not observed

[&]The data are from (24).